Computational Materials Science 52 (2012) 268–273

Contents lists available at ScienceDirect

Computational Materials Science

journal homepage: www.elsevier.com/locate/commatsci

A three-dimensional finite element for gradient elasticity based on a mixed-type formulation

L. Zybell [a,*], U. Mühlich [a], M. Kuna [a], Z.L. Zhang [b]

[a] TU Bergakademie Freiberg, Institute of Mechanics and Fluid Dynamics, Lampadiusstr. 4, D-09596 Freiberg, Germany
[b] Norwegian University of Science and Technology (NTNU), Department of Structural Engineering, Richard Birkelands vei 1a, N-7491 Trondheim, Norway

ARTICLE INFO

Article history:
Received 12 November 2010
Received in revised form 18 February 2011
Accepted 20 February 2011
Available online 1 April 2011

Keywords:
Gradient elasticity
Finite elements
Mixed-type formulation

ABSTRACT

This paper presents a novel three-dimensional finite element for gradient elasticity. The new finite element BR153L9 is a straightforward extension of the two-dimensional element QU34L4 developed by Shu et al. (1999) [1], which is based on a mixed-type formulation. Within this paper the derivation of the mixed-type finite element scheme is reviewed and details of the implementation are given. Finally, numerical results of an extended patch test and a benchmark test with the three-dimensional finite element are presented in order to validate the formulation and prove the convergence.

1. Introduction

Gradient elasticity theories as first developed by Toupin [2] and Mindlin [3] have been successfully used for the numerical investigation of size effects, see e.g. Engelen et al. [4] and Mühlich et al. [5]. This is possible, since gradient enhanced models incorporate at least one additional length scale in the constitutive equations, which can be related somehow to microstructural length characteristics. Furthermore, due to its regularization capabilities, gradient elasticity is also suited for the numerical simulation of localization phenomena.

In recent years gradient elasticity theories have received increasing attention. Besides two-dimensional crack problems [6,7], the material behaviour at bi-material interfaces [8] was investigated. Furthermore, gradient elasticity was extended towards anisotropy [9].

The key difficulty in the numerical solution of gradient elastic problems with the finite element (FE) method is the continuity of strains that requires C^1-continuous finite elements. This problem can be avoided by mixed-type formulations using Langrange multipliers [1,10], meshless methods [11] or with a FE formulation in the more general framework of elasticity with microstructure [12], where for all approaches C^0-continuous interpolation suffices. Also C^1-continuous finite elements [13,14] have been recently developed for gradient elasticity. However, there is only a very limited number of existing three-dimensional (3D) finite elements [12,13] for gradient elasticity. To the best of the authors' knowledge, there is no 3D finite element based on a mixed-type formulation in the literature so far.

Within this paper index notation together with the summation convention is used for tensorial quantities. The abbreviation $()_{,i}$ indicates the partial derivative of the considered quantity $()$ with respect to the corresponding spatial coordinate x_i. Furthermore, δ_{ij} is the Kronecker delta and e_{ijk} is the Levi-Civita tensor. Regarding the finite element implementation algebraic vectors and matrices are written in symbolic notation.

2. Strain gradient elasticity

In this section a short introduction to gradient elasticity theories is given first. Then the basic equations of Type-I gradient elasticity are briefly summarized. In the second subsection the constitutive equations for a couple stress material are presented.

2.1. General framework

In the 1960s Mindlin [3] introduced the so called theory of "linear elasticity with microstructure" for a continuum with microstructure based on two different levels of deformation. In the special case of vanishing relative deformation between micro- and macro-level linear elasticity with microstructure degenerates to gradient elasticity. There are three equivalent formulations (Type I, II and III) for gradient elasticity based on the second gradients of displacements, the strain gradients or on the rotation gradients and the symmetric part of the strain gradients. Mindlin and

* Corresponding author.
E-mail address: lutz.zybell@imfd.tu-freiberg.de (L. Zybell).

0927-0256/$ - see front matter © 2011 Elsevier B.V. All rights reserved.
doi:10.1016/j.commatsci.2011.02.026

Eshel [15] showed, that all three formulations are equivalent. Within this paper the Type-I formulation is used exclusively.

The strain energy density function W for a body subjected to mechanical loading can be expressed in terms of the gradient elasticity Type-I formulation as

$$W = W(\varepsilon_{ij}, \tilde{\kappa}_{ijk}) \tag{1}$$

where W depends upon both conventional strains

$$\varepsilon_{ij} = \frac{1}{2}(u_{i,j} + u_{j,i}) \tag{2}$$

and the second-order displacement gradients

$$\tilde{\kappa}_{ijk} = u_{k,ij} \tag{3}$$

The work conjugate quantities to the strains and the second-order displacement gradients are the stresses σ_{ij} and the so called higher-order stresses $\tilde{\mu}_{ijk}$ which are defined as

$$\sigma_{ij} = \frac{\partial W}{\partial \varepsilon_{ij}}, \quad \tilde{\mu}_{ijk} = \frac{\partial W}{\partial \tilde{\kappa}_{ijk}} \tag{4}$$

Applying the principle of virtual work, the following extended equilibrium conditions can be derived for a body which occupies the region $\mathcal{B}$ with the boundary $\partial\mathcal{B}$

$$(\sigma_{ik} - \tilde{\mu}_{jik,j})_{,i} + b_k = 0_k \quad x_k \in \mathcal{B} \tag{5}$$

$$t_k = t_k^* \quad x_k \in \partial\mathcal{B}^{\{t\}} \tag{6}$$

$$r_k = r_k^* \quad x_k \in \partial\mathcal{B}^{\{s\}} \tag{7}$$

where the quantities marked by an asterisk symbol are prescribed values and b_k is a body force vector. The components of the traction vector t_k and the higher-order traction vector r_k are given as follows:

$$t_k = n_i(\sigma_{ik} - \tilde{\mu}_{jik,j}) + n_i n_j \tilde{\mu}_{ijk}(D_p n_p) - D_j(n_i \tilde{\mu}_{ijk}) \tag{8}$$

$$r_k = n_i n_j \tilde{\mu}_{ijk} \tag{9}$$

In the above equations $D_j(.) = (\delta_{jk} - n_j n_k)\frac{\partial(.)}{\partial x_k}$ is a surface gradient operator and n_i is the ith component of the unit surface normal vector. Following Mindlin [3], there are also forces along the edges of the body. Due to the fact, that these so called "edge forces" are zero in all numerical examples considered within this paper, they are omitted in the following for the sake of brevity.

The full set of equations for gradient elasticity consists of the equilibrium conditions (5), the kinematic relations (2), (3) and the constitutive equations (4), which will be discussed in more detail within the next subsection. Furthermore, besides the natural boundary conditions (6) the following essential boundary conditions are necessary to define the boundary value problem completely

$$u_k = u_k^* \quad x_k \in \partial\mathcal{B}^{\{u\}} \tag{10}$$

$$(Du_k) = (Du_k)^* \quad x_k \in \partial\mathcal{B}^{\{\psi\}} \tag{11}$$

where $D(.) = n_k \partial(.)/\partial x_k$ is a surface normal gradient operator.

2.2. Constitutive equations

The general quadratic form of the strain energy density function for an isotropic linear strain gradient elastic material can be written as

$$W = \frac{1}{2}\varepsilon_{ij} C_{ijkl} \varepsilon_{kl} + \frac{1}{2}\tilde{\kappa}_{ijk} D_{ijklmn} \tilde{\kappa}_{lmn} \tag{12}$$

where C_{ijkl} is the classical fourth-order elasticity tensor depending on the standard Lamé constants μ and λ. The sixth-order material tensor D_{ijklmn} relates second-order displacement gradients $\tilde{\kappa}_{ijk}$ and higher-order stresses $\tilde{\mu}_{ijk}$ and depends on five independent material parameters $a_1 \cdots a_5$ of dimension stress times length squared. So the strain energy density function can be rewritten as [3]

$$W = \frac{1}{2}\lambda\varepsilon_{ii}\varepsilon_{jj} + \mu\varepsilon_{ij}\varepsilon_{ij} + a_1\tilde{\kappa}_{ijj}\tilde{\kappa}_{ikk} + a_2\tilde{\kappa}_{iik}\tilde{\kappa}_{kjj} + a_3\tilde{\kappa}_{iik}\tilde{\kappa}_{jjk} + a_4\tilde{\kappa}_{ijk}\tilde{\kappa}_{ijk} + a_5\tilde{\kappa}_{ijk}\tilde{\kappa}_{kji} \tag{13}$$

For simplicity, a couple stress material [1], which is a special case of gradient elasticity, with the following strain energy density function was used within this investigation:

$$W = \frac{1}{2}\lambda\varepsilon_{ii}\varepsilon_{jj} + \mu\varepsilon_{ij}\varepsilon_{ij} + 2\mu l^2 \chi_{ij}\chi_{ij} \tag{14}$$

Here, the curvature χ_{ij} of a material point is related to its rotation θ_i by $\chi_{ij} = \theta_{i,j} = \frac{1}{2}e_{ipk}u_{k,pj}$ and l is the internal material length scale entering the constitutive equations. Finally, this results in $a_1 = a_2 = a_3 = 0$ and $a_4 = -a_5 = \frac{1}{2}\mu l^2$ for the coefficients a_n in (13) and the constitutive equations for the couple stress material read

$$\sigma_{ij} = \lambda\delta_{ij}\varepsilon_{kk} + 2\mu\varepsilon_{ij} \tag{15}$$

$$\tilde{\mu}_{ijk} = \mu l^2(\tilde{\kappa}_{ijk} - \tilde{\kappa}_{kji}) \tag{16}$$

3. Mixed-type finite element formulation

The derivation of a weak form from the equilibrium equations (5) and its finite element implementation would require $C^{(1)}$-continuous finite elements. In order to reduce the continuity requirements, Shu et al. [1] developed a mixed-type formulation based on Lagrange multipliers.

Within this formulation additional degrees of freedom DOF ψ_{ij}, the so called relaxed strains, are introduced and equality with the displacement gradients is postulated in an approximate manner

$$\psi_{ij} - u_{j,i} \approx 0_{ij} \tag{17}$$

Furthermore, the relaxed strain gradients are defined by

$$\eta_{ijk} = \frac{1}{2}(\psi_{jk,i} + \psi_{ik,j}) \tag{18}$$

Rewriting the constitutive relations regarding the higher-order stresses (16) with the relaxed strain gradients η_{ijk} instead of the second-order displacement gradients $\tilde{\kappa}_{ijk}$ yields the approximations τ_{ijk} of the higher-order stresses

$$\tau_{ijk} = \mu l^2(\eta_{ijk} - \eta_{kji}) \tag{19}$$

The usage of new kinematic quantities affects as well the equilibrium conditions (5). By introducing the Lagrange multipliers

$$\rho_{ik} = -\tilde{\mu}_{jik,j} \tag{20}$$

the equilibrium conditions (5) become

$$(\sigma_{ik} + \rho_{ik})_{,i} + b_k = 0_k \quad x_k \in \mathcal{B} \tag{21}$$

and the equality of the divergence of higher-order stresses $\tilde{\mu}_{jik}$ and its approximations τ_{ijk} can be enforced by

$$\tau_{jik,j} + \rho_{ik} \approx 0_{ik} \tag{22}$$

In order to use finite elements the corresponding weak form of the mixed formulation can be obtained by multiplying (21), (22) and (17) with proper test functions and integrating over the volume $\mathcal{B}$ of the considered body. This leads to the following system of equations involving only first-order gradients of kinematic quantities:

$$\int_{\mathcal{B}} \left((\sigma_{jk} + \rho_{jk})_{,j} + b_k\right)\delta u_k \mathrm{d}V = 0 \tag{23}$$

$$\int_{\mathcal{B}} (\tau_{ijk,i} + \rho_{jk})\delta\psi_{jk}\mathrm{d}V = 0 \tag{24}$$

$$\int_{\mathcal{B}} (-u_{k,j} + \psi_{jk})\delta\rho_{jk}\mathrm{d}V = 0 \tag{25}$$

where there is no sum over j and k in Eq. (25).

Rewriting Eqs. (23) and (24) by making use of Gauss' as well as Stokes' theorem, introducing the boundary conditions (6) and (7) on $\partial\mathcal{B}^{[t]}$ and $\partial\mathcal{B}^{[s]}$ and assuming that the virtual displacements δu_i and relaxed strains $\delta\psi_{ij}$ vanish on $\partial\mathcal{B}^{\{u\}}$ and $\partial\mathcal{B}^{\{\psi\}}$, resp., yields the final virtual work equations

$$\int_{\mathcal{B}} \left(\sigma_{ij}\delta\varepsilon_{ij} - \rho_{jk}\delta u_{k,j}\right)\mathrm{d}V = \int_{\mathcal{B}} b_k\delta u_k\mathrm{d}V + \int_{\partial\mathcal{B}^{\{t\}}} t_k\delta u_k\mathrm{d}A \tag{26}$$

$$\int_{\mathcal{B}} \left(\tau_{ijk}\delta\eta_{ijk} + \rho_{jk}\delta\psi_{jk}\right)\mathrm{d}V = \int_{\partial\mathcal{B}^{\{s\}}} s_{jk}\delta\psi_{jk}\mathrm{d}A \tag{27}$$

$$\int_{\mathcal{B}} (-u_{k,j} + \psi_{jk})\delta\rho_{jk}\mathrm{d}V = 0 \quad \text{(no sum over } j \text{ and } k\text{)} \tag{28}$$

where the second-order tensor $s_{jk} = n_j r_k$ is used for later conveniences.

4. Finite element implementation

In this section a straightforward extension of the two-dimensional finite element QU34L4 introduced by Shu et al. [1] into the three-dimensional finite element BR153L9 is presented. The numerically best performing finite element QU34L4 from [1] was chosen to develop the corresponding three-dimensional element, what was already suggested in [13]. In this section the new element BR153L9 will be presented first. Then Voigt notation is introduced for the kinematic quantities, the constitutive relations and the modified virtual work equation and finally some remarks related to the finite element implementation are given.

The new developed isoparametric brick element BR153L9 (see Fig. 1) is a so called Lagrangian finite element. It contains 27 nodes and the total number of degrees of freedom (DOF) is 162. There are twelve DOF u_i and ψ_{ij} at each corner node and three DOF u_i at each of the remaining 19 nodes. Additionally, the element uses nine Lagrange multipliers ρ_{ij} which are assumed to be constant throughout the element and which are connected to the middle node. The displacements u_i are interpolated by the conventional triquadratic Langrangian shape functions (see e.g. [16]) and the relaxed strains ψ_{ij} are interpolated trilinearly (see e.g. [17]).

Introducing Voigt notation within the FE scheme, the displacements $\mathbf{u}$, the relaxed strains $\boldsymbol{\psi}$, and the Lagrange multipliers $\boldsymbol{\rho}$ read

$$\mathbf{u} = \{u_1\, u_2\, u_3\}^{\mathrm{T}} = \mathbf{N}^{[u]^{\mathrm{T}}}\hat{\mathbf{u}} \tag{29}$$

$$\boldsymbol{\psi} = \{\psi_{11}\,\psi_{22}\,\psi_{33}\,\psi_{21}\,\psi_{12}\,\psi_{31}\,\psi_{13}\,\psi_{32}\,\psi_{23}\}^{\mathrm{T}} = \mathbf{N}^{[\psi]^{\mathrm{T}}}\hat{\boldsymbol{\psi}} \tag{30}$$

$$\boldsymbol{\rho} = \{\rho_{11}\,\rho_{22}\,\rho_{33}\,\rho_{21}\,\rho_{12}\,\rho_{31}\,\rho_{13}\,\rho_{32}\,\rho_{23}\}^{\mathrm{T}} = \mathbf{N}^{[\rho]^{\mathrm{T}}}\hat{\boldsymbol{\rho}} \tag{31}$$

where $\mathbf{N}^{[u]}$, $\mathbf{N}^{[\psi]}$ and $\mathbf{N}^{[\rho]}$ are matrices of shape functions while $\hat{\mathbf{u}}$, $\hat{\boldsymbol{\psi}}$ and $\hat{\boldsymbol{\rho}}$ are nodal degrees of freedom. The derivatives of the kinematic quantities, the displacement gradients $\nabla\mathbf{u}$, the strains $\boldsymbol{\varepsilon}$ and the relaxed strain gradients $\boldsymbol{\eta}$ are given by

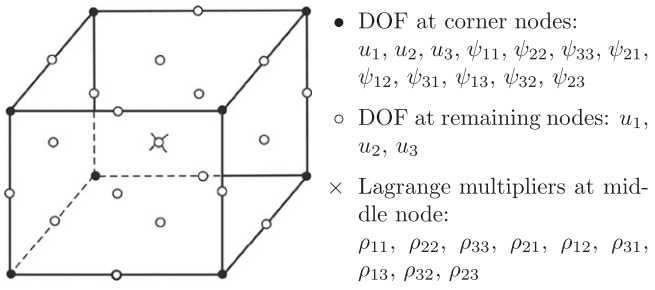

Fig. 1. Sketch of element BR153L9 and order of DOF u_i and ψ_{ij} and Lagrange multipliers ρ_{ij} at nodes.

$$\nabla\mathbf{u} = \{u_{1,1}\,u_{2,2}\,u_{3,3}\,u_{1,2}\,u_{2,1}\,u_{1,3}\,u_{3,1}\,u_{2,3}\,u_{3,2}\}^{\mathrm{T}} = \mathbf{M}^{[u]^{\mathrm{T}}}\hat{\mathbf{u}} \tag{32}$$

$$\boldsymbol{\varepsilon} = \{\varepsilon_{11}\,\varepsilon_{22}\,\varepsilon_{33}\,\varepsilon_{12}\,\varepsilon_{13}\,\varepsilon_{23}\}^{\mathrm{T}} = \mathbf{B}^{[u]^{\mathrm{T}}}\hat{\mathbf{u}} \tag{33}$$

$$\boldsymbol{\eta} = \{\eta_{111}\,\eta_{222}\,\eta_{333}\,\eta_{112}\,\eta_{121}\,\eta_{122}\,\eta_{221}\,\eta_{113}\cdots \eta_{331}\,\eta_{223}\cdots\eta_{332}\,\eta_{123}\,\eta_{132}\,\eta_{321}\}^{\mathrm{T}} = \mathbf{B}^{[\psi]^{\mathrm{T}}}\hat{\boldsymbol{\psi}} \tag{34}$$

In the above equations the matrices $\mathbf{M}^{[u]}$, $\mathbf{B}^{[u]}$ and $\mathbf{B}^{[\psi]}$ contain first order derivatives of the shape funtions of DOF $\mathbf{u}$ and $\boldsymbol{\psi}$ in the required order.

The constitutive equations read in vector form

$$\boldsymbol{\sigma} = \{\sigma_{11}\,\sigma_{22}\,\sigma_{33}\,\sigma_{12}\,\sigma_{13}\,\sigma_{23}\}^{\mathrm{T}} = \mathbf{C}\boldsymbol{\varepsilon} \tag{35}$$

$$\boldsymbol{\tau} = \{\tau_{111}\,\tau_{222}\,\tau_{333}\,\tau_{112}\,\tau_{121}\,\tau_{122}\,\tau_{221}\,\tau_{113}\ldots\tau_{331}\,\tau_{223}\ldots \tau_{332}\,\tau_{123}\,\tau_{132}\,\tau_{321}\}^{\mathrm{T}} = \mathbf{D}\boldsymbol{\eta} \tag{36}$$

where $\mathbf{C}$ and $\mathbf{D}$ are the elasticity and the higher-order elasticity matrix, respectively.

Assuming zero body forces $\mathbf{b} = \mathbf{0}$, the virtual work Equations. (26)–(28) can be rewritten in Voigt notation

$$\int_{\mathcal{B}} (\delta\boldsymbol{\varepsilon}^{\mathrm{T}}\boldsymbol{\sigma} - \nabla\delta\mathbf{u}^{\mathrm{T}}\boldsymbol{\rho})\mathrm{d}V = \int_{\partial\mathcal{B}^{\{t\}}} \delta\mathbf{u}^{\mathrm{T}}\mathbf{t}\mathrm{d}A \tag{37}$$

$$\int_{\mathcal{B}} (\delta\boldsymbol{\eta}^{\mathrm{T}}\boldsymbol{\tau} + \delta\boldsymbol{\psi}^{\mathrm{T}}\boldsymbol{\rho})\mathrm{d}V = \int_{\partial\mathcal{B}^{\{s\}}} \delta\boldsymbol{\psi}^{\mathrm{T}}\mathbf{s}\mathrm{d}A \tag{38}$$

$$\int_{\mathcal{B}} \delta\boldsymbol{\rho}^{\mathrm{T}}(\boldsymbol{\psi} - \nabla\mathbf{u})\mathrm{d}V = 0 \tag{39}$$

where the known boundary tractions and higher-order boundary tractions are incorporated by

$$\mathbf{t} = \{t_1^*\, t_2^*\, t_3^*\}^{\mathrm{T}} \tag{40}$$

$$\mathbf{s} = \{n_1\, r_1^*\, n_2\, r_2^*\, n_3\, r_3^*\, n_2\, r_1^* n_1 r_2^*\, n_3\, r_1^*\, n_1\, r_3^*\, n_3\, r_2^*\, n_2\, r_3^*\}^{\mathrm{T}} \tag{41}$$

Introducing (29)–(36) into the above equations and some algebraic manipulation yields

$$\delta\hat{\mathbf{u}}^{\mathrm{T}}\left(\int_{\mathcal{B}} \left(\mathbf{B}^{[u]}\boldsymbol{\sigma} - \mathbf{M}^{[u]}\mathbf{N}^{[\rho]^{\mathrm{T}}}\hat{\boldsymbol{\rho}}\right)\mathrm{d}V - \int_{\partial\mathcal{B}^{\{t\}}} \mathbf{N}^{[u]}\mathbf{t}\mathrm{d}A\right) = 0 \tag{42}$$

$$\delta\hat{\boldsymbol{\psi}}^{\mathrm{T}}\left(\int_{\mathcal{B}} \left(\mathbf{B}^{[\psi]}\boldsymbol{\tau} + \mathbf{N}^{[\psi]}\mathbf{N}^{[\rho]^{\mathrm{T}}}\hat{\boldsymbol{\rho}}\right)\mathrm{d}V - \int_{\partial\mathcal{B}^{\{s\}}} \mathbf{N}^{[\psi]}\mathbf{s}\mathrm{d}A\right) = 0 \tag{43}$$

$$\delta\hat{\boldsymbol{\rho}}^{\mathrm{T}}\int_{\mathcal{B}} \mathbf{N}^{[\rho]}\left(\mathbf{N}^{[\psi]^{\mathrm{T}}}\hat{\boldsymbol{\psi}} - \mathbf{M}^{[u]^{\mathrm{T}}}\hat{\mathbf{u}}\right)\mathrm{d}V = 0 \tag{44}$$

Because $\delta\hat{\mathbf{u}}$, $\delta\hat{\boldsymbol{\psi}}$ and $\delta\hat{\boldsymbol{\rho}}$ are independent variations, Eqs. (42)–(44) can be transformed into the following final system of equations:

$$\begin{bmatrix} \mathbf{K}^{[uu]} & \mathbf{0} & -\mathbf{K}^{[u\rho]} \\ \mathbf{0} & \mathbf{K}^{[\psi\psi]} & \mathbf{K}^{[\psi\rho]} \\ -\mathbf{K}^{[u\rho]^{\mathrm{T}}} & \mathbf{K}^{[\psi\rho]^{\mathrm{T}}} & \mathbf{0} \end{bmatrix} \begin{Bmatrix} \hat{\mathbf{u}} \\ \hat{\boldsymbol{\psi}} \\ \hat{\boldsymbol{\rho}} \end{Bmatrix} = \begin{Bmatrix} \mathbf{F}^{[u]} \\ \mathbf{F}^{[\psi]} \\ \mathbf{0} \end{Bmatrix} \tag{45}$$

where the stiffness matrices are

$$\mathbf{K}^{[uu]} = \int_{\mathcal{B}} \mathbf{B}^{[u]}\mathbf{C}\mathbf{B}^{[u]^{\mathrm{T}}}\mathrm{d}V, \quad \mathbf{K}^{[u\rho]} = \int_{\mathcal{B}} \mathbf{M}^{[u]}\mathbf{N}^{[\rho]^{\mathrm{T}}}\mathrm{d}V \tag{46}$$

$$\mathbf{K}^{[\psi\psi]} = \int_{\mathcal{B}} \mathbf{B}^{[\psi]}, \mathbf{D}\mathbf{B}^{[\psi]^{\mathrm{T}}}\mathrm{d}V, \quad \mathbf{K}^{[\psi\rho]} = \int_{\mathcal{B}} \mathbf{N}^{[\psi]}\mathbf{N}^{[\rho]^{\mathrm{T}}}\mathrm{d}V$$

and the right hand side vectors read

$$\mathbf{F}^{[u]} = \int_{\partial\mathcal{B}^{\{t\}}} \mathbf{N}^{[u]}\mathbf{t}\mathrm{d}A, \quad \mathbf{F}^{[\psi]} = \int_{\partial\mathcal{B}^{\{s\}}} \mathbf{N}^{[\psi]}\mathbf{s}\mathrm{d}A \tag{47}$$

The system of equations (45) was implemented for the new element BR153L9 with the corresponding shape functions and their derivatives as a User Element into the commercial FE software Abaqus [18]. The implementation of the 3D finite element in the general nonlinear framework provided by the Abaqus interface UEL was realized analogously to the implementation of the 2D element QU34L4, which is described in detail in [19]. Special attention must

be paid to the zero diagonal terms in the element stiffness matrix in (45). These zero terms cause problems with the Abaqus solver and small numbers must be used instead.

5. Numerical tests

5.1. Patch test

In order to investigate the numerical behaviour of the finite element BR153L9 an extended patch test was performed. In order to fulfill the count test [17] a patch of $2 \times 2 \times 2$ elements was used. The dimension of the patch was chosen to be $1 \times 1 \times 1$ mm^3. Both a regular and a distorted mesh were used for the patch test, see Fig. 2. For the distorted mesh the center node of the patch is located at $x_1 = x_2 = x_3 = 0.6$ mm and the other inner nodes were shifted accordingly.

For both patch tests, with a regular and distorted mesh, the displacements u_i and relaxed strains ψ_{ij} were prescribed at all boundary nodes of the patch and the values at the inner nodes were compared with the given analytical formulation. The prescribed displacement field was chosen to be of quadratic form

$$u_1(x_1,x_2,x_3) = d_1x_1 + d_2x_2 + d_3x_3 + e_1x_1^2 + e_2x_2^2 + e_3x_3^2 + f_1x_1x_2 + f_2x_1x_3 + f_3x_2x_3 \tag{48}$$

$$u_2(x_1,x_2,x_3) = d_4x_1 + d_5x_2 + d_6x_3 + e_4x_1^2 + e_5x_2^2 + e_6x_3^2 + f_4x_1x_2 + f_5x_1x_3 + f_6x_2x_3 \tag{49}$$

$$u_3(x_1,x_2,x_3) = d_7x_1 + d_8x_2 + d_9x_3 + e_7x_1^2 + e_8x_2^2 + e_9x_3^2 + f_7x_1x_2 + f_8x_1x_3 + f_9x_2x_3 \tag{50}$$

The relation between relaxed strains and displacements given by (17) was strictly enforced ($\psi_{ij} = u_{j,i}$) on the boundary of the patch. The resulting relaxed strain field was prescribed on the corresponding boundary nodes of the patch.

For the numerical tests the elastic constants, Young's modulus and Poisson's ratio, were assumed to be $E = 1000$ MPa and $\nu = 0.3$ and the microstructural length was chosen to be $l = 1$ mm. For the zero diagonal terms the value $\alpha = 1.0\text{E}{-10}$ was used and the patch tests were performed for different choices of coefficients d_1 til f_9 for the regular and the distorted mesh. At first, all 27 cases with one single constant different from zero and all other constants equal to zero were investigated. Furthermore, 12 cases with linear combinations of two or three constants different from zero were also considered. For all these variations of coefficients the displacements, strains and stresses and the corresponding higher-order quantities (relaxed strains, relaxed strain gradients and higher-order stresses) were calculated using the FEM at all inner nodes and compared with the analytical solution based on the particular given fields. All tests for both the regular and the distorted patch yield exact results for all investigated quantities (displacements u_i and relaxed strains ψ_{ij} at the middle node, comparison between displacement gradients $u_{j,i}$ and relaxed strains ψ_{ij} at integration points) within round-off errors.

5.2. Benchmark test

In order to study the convergence properties of the new developed finite element BR153L9, the problem of an infinite solid containing a cylindrical hole is investigated. The solid is subjected to remote uniform tension as shown in Fig. 3a. The analytical solution of this two-dimensional problem regarding a couple stress material was found by Mindlin [20]. The stress concentration factor P at the boundary of the hole can be calculated by

$$P = \frac{\sigma_{22}(x_1 = 0, x_2 = a)}{\sigma^\infty} = \frac{3+F}{1+F} \tag{51}$$

where σ^∞ is the remote uniform tension and the function F is given by

$$F = \frac{8(1-\nu)}{4 + \left(\frac{a}{l}\right)^2 + 2\left(\frac{a}{l}\right)\frac{K_0(a/l)}{K_1(a/l)}} \tag{52}$$

Furthermore, a is the radius of the cylindrical hole, l is the internal material length scale, and K_0 and K_1 are the modified Bessel functions of the second kind of order zero and one.

Due to symmetry, only a quarter of the problem has to be modelled within the 3D FE analysis, see Fig. 3b. In order to simulate plane strain conditions, the displacement u_3 must be restricted on both x_3-planes and it is sufficient to use one element layer in x_3-direction. Within the simulations a body with a volume of $30 \times 30 \times 30$ mm was modelled and the hole radius was $a = 1$ mm. The elastic constants were chosen to be $E = 1000$ MPa and $\nu = 0.0$ and $\alpha = 1\text{E}{-10}$ was used for the zero diagonal terms. The internal material length scale was varied ($l = 1.00, 0.10, 0.01$ mm) in order to study its influence on the stress concentration. To prove the convergence of the new finite element BR153L9, three different meshes with increasing mesh density (see Fig. 4) were used within the simulations.

The following boundary conditions were prescribed on the quarter FE model according to Fig. 3b:

- surfaces ABCDE and FGHIJ: $u_3 = 0$ mm, $\psi_{33} = \psi_{13} = \psi_{31} = \psi_{23} = \psi_{32} = 0$,
- surface AEJF: $u_1 = 0$ mm, $\psi_{12} = \psi_{21} = \psi_{13} = \psi_{31} = 0$,
- surface CHID: $u_2 = 0$ mm, $\psi_{12} = \psi_{21} = \psi_{23} = \psi_{32} = 0$,
- surface BCHG: $t_1^* = \sigma^\infty = 1$ MPa.

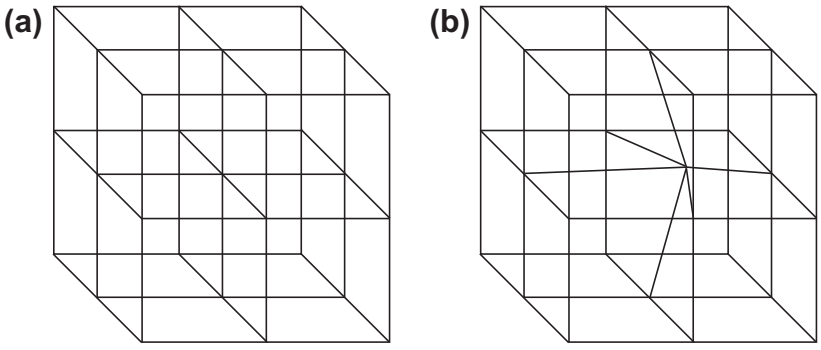

Fig. 2. Regular (a) and distorted (b) meshes used for the patch tests.

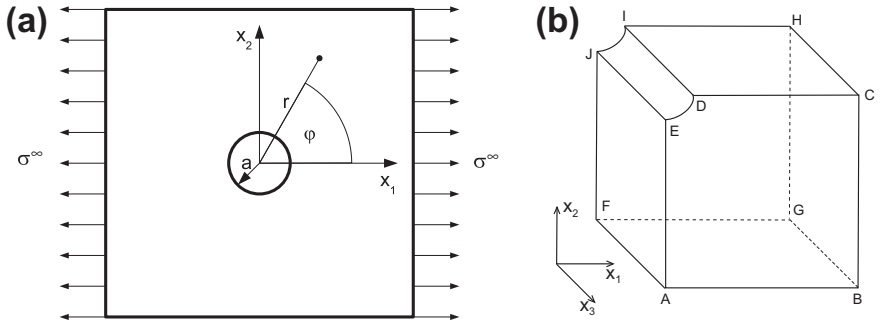

Fig. 3. Geometry and notation of the benchmark test (a) and sketch of the volume used in the FE simulations (b).

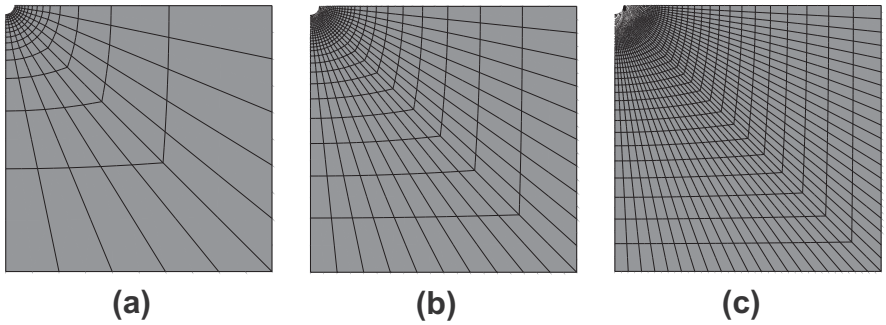

Fig. 4. Front view of the three meshes used in the benchmark test: (a) mesh 1: 2734 nodes, 150 elements (b) mesh 2: 10504 nodes, 600 elements (c) mesh 3: 41164 nodes, 2400 elements.

Table 1
Comparison of stress concentration factors P for the benchmark test between three meshes consisting of the new developed element BR153L9, analytical solution [20] and two-dimensional element QU34L4 [1].

	Mesh 1	Mesh 2	Mesh 3	Analytical	QU34L4
$l = 1.00$	1.938	1.912	1.901	1.889	1.897
$l = 0.10$	2.916	2.895	2.889	2.878	2.894
$l = 0.01$	3.038	3.016	3.010	2.998	3.006

Additionally, on surfaces where neither displacements nor tractions were prescribed, all boundary tractions t_i^* and higher order boundary tractions r_i^* are zero.

The comparison of the stress concentration factors P between the analytical solution [20], the two-dimensional element QU34L4 [1] and simulations with three different meshes consisting of the new developed element BR153L9 is presented in Table 1. The results show clearly, that the stress concentration factors obtained with element BR153L9 converge towards the analytical solution as the mesh density increases. Furthermore, the influence of the internal material length scale l becomes obvious. As long as the ratio between microstructural length scale and hole radius l/a is small, the influence of the strain gradients is negligible. But when l approaches the dimension of a, the stress concentration is diminished. Finally it can be stated, that the new developed finite element BR153L9 has proved to be an efficient formulation for solving boundary value problems for gradient elasticity.

6. Conclusions

In this paper we have presented a three-dimensional finite element for gradient elasticity based on a mixed-type formulation. The new developed finite element BR153L9 is the straightforward extension of the already existing two-dimensional finite element QU34L4 from Shu et al. [1]. The numerical implementation of the new element has been validated by an extended patch test and a benchmark test related to the stress concentration due to a cylindrical hole. The results of the patch test are in excellent agreement with the analytically given fields. Furthermore, a mesh refinement study shows the convergence of the element BR153L9 towards the analytical solution of the benchmark test as the mesh density increases. A comparison of the new element with already existing 3D finite element formulations for gradient elasticity based on other approaches regarding the numerical performance should be envisaged. For this purpose the benchmark test suggested in [13] could be used.

Acknowledgements

Part of this work was done during a visiting stay of the first author at NTNU Trondheim. The financial support of Verbundnetz Gas AG (VNG) for this stay is gratefully acknowledged.

References

[1] J. Shu, W. King, N. Fleck, International Journal for Numerical Methods in Engineering 44 (1999) 373–391.
[2] R. Toupin, Archive for Rational Mechanics and Analysis 11 (1962) 385–414.
[3] R. Mindlin, Archive for Rational Mechanics and Analysis 16 (1964) 51–78.
[4] R. Engelen, N. Fleck, R. Peerlings, M. Geers, International Journal of Solids and Structures 43 (2006) 1857–1877.
[5] U. Mühlich, L. Zybell, M. Kuna, Computational Materials Science 46 (2009) 647–653.
[6] S. Imatani, K. Hatada, G. Maugin, Philosophical Magazine 85 (2005) 4245–4256.
[7] N. Aravas, A. Giannakopoulos, International Journal of Solids and Structures 46 (2009) 4478–4503.
[8] H. Askes, I. Gitman, International Journal of Fracture 156 (2009) 17–222.
[9] I. Gitman, H. Askes, E. Kuhl, E. Aifantis, International Journal of Solids and Structures 47 (2010) 1099–1107.
[10] E. Amanatidou, N. Aravas, Computer Methods in Applied Mechanics and Engineering 191 (2002) 1723–1751.
[11] H. Askes, E. Aifantis, International Journal of Fracture 117 (2002) 347–358.

[12] A. Zervos, International Journal for Numerical Methods in Engineering 73 (2008) 564–595.
[13] S. Papanicolopulos, A. Zervos, I. Vardoulakis, International Journal for Numerical Methods in Engineering 77 (2009) 1396–1415.
[14] P. Fischer, J. Mergheim, P. Steinmann, International Journal for Numerical Methods in Engineering 82 (2010) 1282–1307.
[15] R. Mindlin, N. Eshel, International Journal of Solids and Structures 4 (1968) 109–124.
[16] C. Grummitt, G. Baker, Theoretical and Applied Fracture Mechanics 32 (1999) 189–201.
[17] O. Zienkiewicz, R. Taylor, J. Zhu, The Finite Element Method: Its Basis and Fundamentals, Elsevier Butterworth Heinemann, 2005.
[18] Simulia, Abaqus Version 6.8 Documentation, Dassault systèmes, 2008.
[19] L. Zybell, Implementation of a user element considering strain gradient effects into the FE-program Abaqus, Master's Thesis, TU Bergakademie Freiberg, 2007.
[20] R. Mindlin, Experimental Mechanics 3 (1963) 1–7.